



Optics Letters

Submillimeter-spatial-resolution φ -OFDR strain sensor using femtosecond laser induced permanent scatters

YANJIE MENG,^{1,2} CAILING FU,^{1,2,*}  LIN CHEN,^{1,2} CHAO DU,^{1,2} HUAJIAN ZHONG,^{1,2} YIPING WANG,^{1,2}  JUN HE,^{1,2}  AND WEIJIA BAO^{1,2}

¹Key Laboratory of Optoelectronic Devices and Systems of Ministry of Education/GuangDong Province, College of Physics and Optoelectronic Engineering, Shenzhen University, Shenzhen 518060, China

²Shenzhen Key Laboratory of Photonic Devices and Sensing Systems for Internet of Things, Guangdong and Hong Kong Joint Research Centre for Optical Fibre Sensors, Shenzhen University, Shenzhen 518060, China

*Corresponding author: fucailing@szu.edu.cn

Received 22 September 2022; revised 7 November 2022; accepted 7 November 2022; posted 9 November 2022; published 1 December 2022

A φ -optical frequency domain reflectometry (OFDR) strain sensor with a submillimeter-spatial-resolution of 233 μm is demonstrated by using femtosecond laser induced permanent scatters (PSs) in a standard single-mode fiber (SMF). The PSs-inscribed SMF, i.e., strain sensor, with an interval of 233 μm exhibited a Rayleigh backscattering intensity (RBS) enhancement of 26 dB and insertion loss of 0.6 dB. A novel, to the best of our knowledge, method, i.e., PSs-assisted φ -OFDR, was proposed to demodulate the strain distribution based on the extracted phase difference of P- and S-polarized RBS signal. The maximum measurable strain was up to 1400 $\mu\epsilon$ at a spatial resolution of 233 μm . © 2022 Optica Publishing Group

<https://doi.org/10.1364/OL.476349>

Distributed optical fiber sensing has found various applications in structural health monitoring, and biomedical and clinical measurements due to its advantages, including but not limited to a high sensitivity and resolution for many physical parameters [1]. Compared with the spatial resolution at the cm-level of time-expanded phase-sensitive optical time-domain reflectometry (OTDR) [2] or Brillouin optical correlation domain analysis (BOCDA) [3], optical frequency domain reflectometry (OFDR) is widely known for its mm-level spatial resolution [4,5]. Currently, two types of demodulation methods based on OFDR have been proposed, i.e., spectrum-based OFDR using spectrum shift, and φ -OFDR using phase [6,7]. The sensing performance of spectrum-based OFDR is limited by the weak Rayleigh backward scattering (RBS) signal in the fiber. Several methods have been proposed to enhance the RBS intensity, such as using a gold-nanoparticles-doped [8] or UV-exposed silica fiber [9], or femtosecond laser induced nano-gratings [4], grating arrays [10], and point reflectors [11,12]. Unfortunately, the spatial resolution for spectrum-based OFDR has remained at the mm-level even with the RBS enhancement of 40 dB, which results from the following two factors. On the one hand, the optical frequency resolution that determines the accuracy of strain

sensing is limited by the sample number in the sliding window [4]. On the other hand, spatial segment mismatch caused by large fiber deformation leading to spectrum similarity reduction further hinders the wide strain measurement range [5]. Unlike spectrum-based OFDR, φ -OFDR has the potential to achieve higher resolution because no sliding window is imposed on the spatial domain signal. In addition to dealing with the weak RBS as the same as the spectrum-based OFDR, the strain sensing range was also difficult to extend due to the mismatch of the spatial segment.

Recently, femtosecond laser induced reflectors in the fiber have been used to realize distributed sensing. Redding *et al.* presented a low-noise φ -OTDR distributed acoustic sensor using localized point reflectors [11]. Then a Fabry–Perot interferometer array formed by point reflectors was demonstrated for chemical sensing based on OFDR [12]. Enhanced RBS lines fabricated by reel-to-reel femtosecond laser direct writing technology were also used to improve the temperature sensing performance of spectrum-based OFDR [4]. Thus, the spatial resolution of the OFDR could be further improved based on femtosecond laser induced microstructures.

In this Letter, a φ -OFDR strain sensor with a submillimeter spatial resolution, i.e., 233 μm , was demonstrated by using the femtosecond laser induced permanent scatters (PSs) in a standard single-mode fiber (SMF), i.e., PSs-inscribed SMF. The amplitude enhancement characteristics of the P- and S-polarized RBS signals for the PSs-inscribed SMF were studied. Phase differences extracted by traditional φ -OFDR and the PSs-assisted φ -OFDR method were compared. Moreover, the detailed process to demodulate the strain distribution by using the PSs-assisted φ -OFDR method was also studied.

As shown in Fig. 1(a), the PSs were inscribed in a standard SMF by using femtosecond laser direct writing technology. The pulse width and wavelength of the femtosecond laser was 290 fs and 513 nm, respectively, and the repetition rate could be tuned from single shot to 200 kHz. A single-pulse laser with an

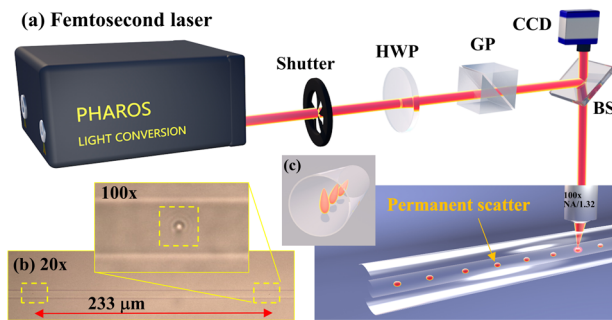


Fig. 1. (a) Schematic diagram of permanent scatterers (PSs) inscribed in standard single-mode fiber (SMF) by a femtosecond laser direct writing technique. HWP, half-wave plate; GP, Glan-prism polarizer; BS, beam splitter. (b) Microscopy images of obtained PS with 20 \times and 100 \times objective lens. (c) Schematic of the incompletely paralleled PSs.

energy of 1.75 μJ was focused in the SMF core via a 100 \times oil-immersion objective to inscribe PSs. A 200.38-mm-long PSs-inscribed SMF with a number of 860 PSs was obtained, where the interval between two PSs was 233 μm . As shown in Fig. 1(b), the size of the obtained PSs without physical damage was less than one-tenth of the core diameter.

A conventional OFDR was used to acquire the P-polarized and S-polarized RBS signal of the PSs-inscribed SMF. (See Supplement 1 for more information about the experimental setup.) As shown in Figs. 2(a) and 2(b), the average amplitude enhancement and insertion loss (IL) of P-polarized and S-polarized RBS signal were approximately 26 dB and 0.6 dB, respectively. Then the average IL induced by each PS was 0.0007 dB. However, the amplitude enhancement consistency of the P-polarized RBS signal was higher than that of the S-polarized RBS signal. The reason was that the polarization angle of the PSs-inscribed SMF was varied from 62.5 $^\circ$ to 89.8 $^\circ$, as shown in Fig. 2(c), resulting from the conical shape of the PSs [13] and incompletely paralleled PSs illustrated in Fig. 1(c). Note that the IL was estimated by subtracting the reflection amplitude of light passing through the PS-inscribed SMF from that before the first PS. In addition, the first PS was located at the position of 10.42 m to avoid multiple reflection cross talk.

The traditional φ -OFDR method was first used to demodulate the strain distribution along the fiber, namely sections I and II in Fig. S1 of Supplement 1, by extracting the phase difference of the P- and S-polarized RBS signals, when the strain was increased from 10 to 50 $\mu\epsilon$ with a step of 10 $\mu\epsilon$ by moving the translation stage on the right. Note that section I was a plain SMF without any treatment, while section II was the PSs-inscribed SMF. Compared with the chaotic phase difference extracted from the plain SMF, the phase difference extracted from the PSs-inscribed SMF exhibited relatively clear periodic phase stripes, when the applied strain was 10 $\mu\epsilon$, as illustrated in Fig. 3. The extracted phase differences under a strain of 20, 30, 40, and 50 $\mu\epsilon$ are shown in Fig. S2 of Supplement 1. This indicated that the strain distribution of the PSs-inscribed SMF could be roughly demodulated by using the traditional φ -OFDR method, attributing to the stronger reflection amplitude of RBS of the PSs-inscribed SMF than that of the plain SMF. However, some outliers of the obtained phase difference were also observed for the PSs-inscribed SMF. The reason is that for the PSs-inscribed SMF, the RBS could only be enhanced at the position with PSs, while the

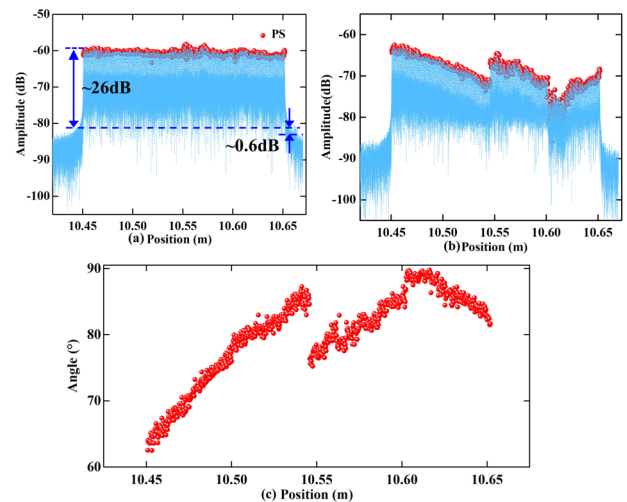


Fig. 2. Measured RBS signals of (a) P-polarized and (b) S-polarized in the distance domain; (c) polarization angle of PSs calculated from the arctangent of P-polarized and S-polarized signal amplitude.

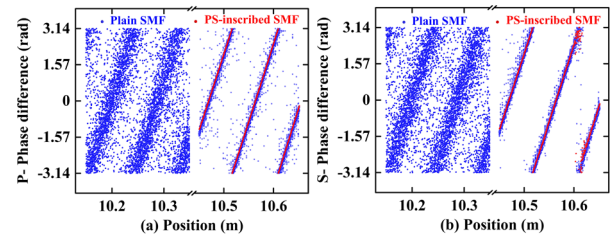


Fig. 3. Extracted phase difference of the (a) P-polarized and (b) S-polarized RBS signals for the plain SMF, i.e., section I, and PSs-inscribed SMF, section II, by using the conventional φ -OFDR method, when the applied strain was 10 $\mu\epsilon$.

signal-to-noise ratio (SNR) of the region between PSs was still low, resulting in phase difference deterioration, i.e., outliers of the obtained phase difference. Therefore, an improved method, i.e., PSs-assisted φ -OFDR, using only the phase difference of the PSs was proposed to demodulate the strain distribution along the fiber.

It is well known that the basic method for converting a time domain signal to a frequency domain signal, i.e., distance domain signal, is the fast Fourier transform (FFT). Although the amplitude of the signal at the position of the PSs was significantly stronger than that without PSs nearby, the phase at the position of the PSs could be more accurately retrieved than at that without PSs. However, spectrum leakage induced by mismatch between beat frequency and sampling frequency would produce false peaks nearby the PSs, leading to a false PSs position. Zero padding is widely used to overcome spectrum leakage, but it requires a larger storage size and calculation time. Therefore, the Chirp z-transform was proposed to convert the time domain signal of the strain sensor to a frequency domain signal instead of conventional FFT. The Chirp-z transform could not only achieve zero-padding, but also have smaller computational load and reduce the calculation time [14].

The detailed process to obtain the strain distribution along the PSs-inscribed SMF was divided into four steps, when the strain was increased from 100 to 1400 $\mu\epsilon$ with a step of 100 $\mu\epsilon$.

Step 1: Using the Chirp z-transform to obtain P- and S-polarized RBS signal in the distance domain. Take the P-polarized RBS signal as an example, the obtained distance domain signals $P(z_k)$ transformed by the Chirp z-transform are expressed as

$$P(z_k) = \sum_{n=0}^{N-1} p(n)z^{-n}, \quad (1)$$

$$z = A \cdot W^{-k}, \quad (2)$$

where $p(n)$ is the sampled time domain signals in P-polarization, and A and W are arbitrary numbers of the following forms:

$$A = e^{j2\pi \cdot \frac{P_{start}}{mL}}, \quad (3)$$

$$W = e^{-j2\pi \cdot \frac{P_{end} - P_{start}}{mL}}, \quad (4)$$

where P_{start} and P_{end} are the start and end position of the strain sensor; m is the number of zero-padding signals; and L is the total length of the SMF, which is defined as the product of sample number and raw spatial resolution.

In addition, the raw spatial resolution δx could be given by

$$\delta x = \frac{\lambda^2}{2 \cdot n_{eff} \cdot \Delta \lambda}, \quad (5)$$

where λ and $\Delta \lambda$ are the central wavelength and sweep range of the TLS; n_{eff} is the refractive index of the medium. In the experiment, the wavelength of the TLS was swept from 1539.45 to 1560.58 nm with a sweep rate of 100 nm/s, corresponding to a spatial resolution of 38.9 μm . When the Chirp-z transform was applied, the calculation spatial resolution, i.e., $\delta x'$, could be redefined by

$$\delta x' = \frac{P_{end} - P_{start}}{m}, \quad (6)$$

In the experiment, the values of P_{start} , P_{end} , and m were 10.42 m, 10.67 m, and 2^{22} , respectively. Therefore, the calculation spatial resolution was calculated to be 59.6 nm.

Step 2: Extracting the phase difference by calculating the angle of between two vectors of reference and measurement signal. Note that the reference signal was defined as the obtained RBS when there was no strain, and the measurement signal was the measured RBS when the strain was applied to the PSs-inscribed SMF. To obtain a more robust phase difference, the angle could be calculated by

$$\Delta \varphi = a \tan 2\{\det[P_{ref}^T, P_{meas}^T], \text{dot}(P_{ref}, P_{meas})\}. \quad (7)$$

where atan2 is the four-quadrant inverse tangent; P_{ref} and P_{meas} are the reference and measurement complex signal in the distance domain, which could be expressed as a two-dimensional vector; \det and dot were used to calculate the determinant of the square matrix and dot product of two vectors, respectively. The

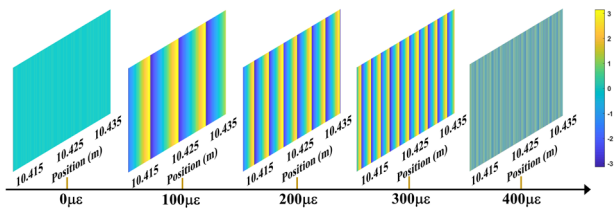


Fig. 4. Evolution of the extracted phase difference of the P-polarized signal when the applied strain was increased from 0 to 400 μe with a step of 100 μe .

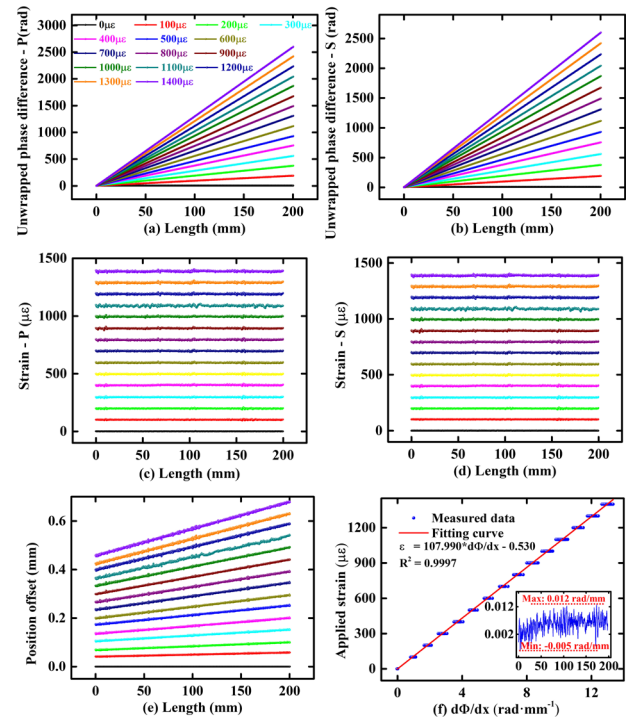


Fig. 5. Unwrapped phase difference of (a) P-polarized and (b) S-polarized RBS signal extracted from the wrapped phase difference; (c),(d) corresponding to strain distribution derived from unwrapped phase difference; (e) calculated position offset of the PSs under different strains; (f) fitting curve of applied strain as a function of differential relative phase. Inset shows the differential relative phase noise.

evolution of the extracted phase difference of the P-polarized signal using Eq. (7) is illustrated in Fig. 4. The extracted phase differences from 500 to 1400 μe are shown in Fig. S3 of Supplement 1. It is obvious that the periodicity of the fringes became denser with the increase of the applied strain.

Step 3: Performing a phase unwrapping operation on the phase difference extracted from the P- and S-polarized signals in step 2 to obtain the unwrapped phase difference. As shown in Figs. 5(a) and 5(b), the unwrapped phase difference, i.e., $\Delta \Phi$, was increased with the increase of the applied strain. The position offset of these permanent scatters was also calculated as shown in Fig. 5(e). Due to the position offset, directly subtracting two phase angle terms of the measurement and reference signal at the same position to obtain the phase difference would induce a large error. However, the position of each PS could be accurately distinguished, which makes it feasible to align the sensing points.

Step 4: Demodulating the strain along the PSs-inscribed SMF based on the unwrapped phase difference in step 3. The strain could be given by [6]

$$\varepsilon = \frac{d\Delta \Phi}{dx} \cdot \frac{\lambda}{4\pi \cdot n_{eff}(1 - P_e)}. \quad (8)$$

where $\Delta \Phi$ is the unwrapped phase difference in step 3; dx is the interval between two PSs, i.e., $dx = 233 \mu\text{m}$; P_e is the elasto-optic coefficient and equal to 0.22. According to Eq. (8), the applied strain could be derived from the unwrapped phase difference of the P- and S-polarized signal. As shown in Figs. 5(c) and

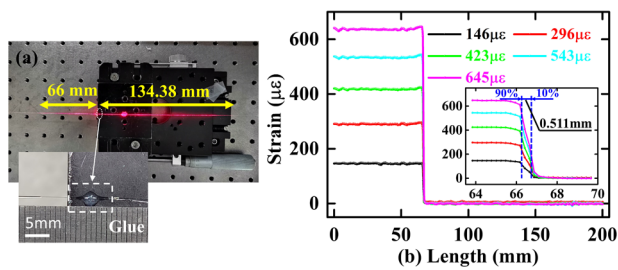


Fig. 6. (a) Experimental setup to verify the spatial resolution, where a 66-mm-long PSs-inscribed SMF between two translation stages was under strain; (b) demodulated strain profile when the strain was increased from 146 $\mu\epsilon$ to 645 $\mu\epsilon$. Inset shows the zoom in of the transition zone.

5(d), the strain demodulated by using the PSs-assisted φ -OFDR method was consistent with the applied strain, which proved the effectiveness of the proposed method. Moreover, the mean errors of the demodulated strain of P-polarized and S-polarized signal were 2.85 $\mu\epsilon$ and 2.91 $\mu\epsilon$, respectively. As shown in Fig. 5(f), the calibrated strain sensitivity was 107.990 $\mu\epsilon/(\text{rad}\cdot\text{mm}^{-1})$, which was almost the same as that of the calculated value from Eq. (8), i.e., 108.696 $\mu\epsilon/(\text{rad}\cdot\text{mm}^{-1})$. In addition, the minimum measurable strain could be obtained by calculating the maximum differential relative phase noise under zero strain. As shown the inset of Fig. 5(f), the maximum phase noise was 0.012 rad/mm, indicating that the minimum measurable strain was 1.30 $\mu\epsilon$.

Finally, the spatial resolution of the strain sensor, i.e., PSs-inscribed SMF, was evaluated by using 10–90% rising length of a transition point [1]. As shown in Fig. 6(a), a 66-mm-long PSs-inscribed SMF between two translation stages was under strain, and the remaining 134.38 mm was immune to strain. Note that the fiber coating of the gluing zone was stripped off. When the strain was increased from 146 $\mu\epsilon$ to 645 $\mu\epsilon$, the strain distribution was successfully demodulated. As shown in Fig. 6(b), the rising length was 0.511 mm, which was greater than the interval between two PSs, i.e., 233 μm . The reason is that the epoxy resin would flow along the fiber, resulting in a loosening bond between the fiber and translation stage. Therefore, the strain change in the transition zone was still gradual rather than jumping. The effect of experiment conditions cannot be neglected especially for sub-millimeter resolution.

The maximum applied strain was limited by the absolute value of the phase change between successive phase differences, i.e., within π radians. When the phase difference was π , the maximum measurable strain could be calculated by

$$\epsilon_{\max} = \frac{340.27 \text{ nm}}{dx}. \quad (9)$$

Then the maximum measurable strain was 1460 $\mu\epsilon$ when the interval of the PSs, i.e., dx , was 233 μm . The maximum measurable strain could be tuned by adjusting the interval of the PSs. When the interval was ranged from one to ten times the spatial resolution, i.e., from dx to $10dx$, the RBS signal was measured. As shown in Fig. S4 of Supplement 1, the PSs could be distinguished at twice the spatial resolution, i.e., $2dx$, and the maximum measurable strain could be increased to 4378 $\mu\epsilon$. However, the IL would be increased with the increase of the number of PSs, which would shorten the sens-

ing length. Therefore, the interval of 233 μm , i.e., $6dx$, was selected to achieve the strain demodulation by using PSs-assisted φ -OFDR.

In conclusion, we have proposed and demonstrated a submillimeter-spatial-resolution φ -OFDR strain sensor based on an RBS-enhanced standard SMF with PSs. A series of PSs with an interval of 233 μm was inscribed in the 200.38-mm-long SMF by femtosecond laser direct writing technology, where the enhancement and insertion loss were approximately 26 dB and 0.6 dB. A novel method, i.e., PSs-assisted φ -OFDR, was proposed to demodulate the strain distribution by extracting the phase difference of each PS at the position of the PSs. The maximum measurable strain of the PSs-inscribed SMF based on PSs-assisted φ -OFDR was 1400 $\mu\epsilon$ with a spatial resolution of 233 μm , i.e., the interval of PSs.

Funding. National Natural Science Foundation of China (nos. 61905155, U1913212); Natural Science Foundation of Guangdong Province (nos. 2019B1515120042, nos. 2021A1515011925); Science, Technology and Innovation Commission of Shenzhen Municipality (20200810121618001, JCYJ20200109114020865, JCYJ20200109114201731, JSGG20201102152200001); Shenzhen Key Laboratory of Photonic Devices and Sensing Systems for Internet of Things.

Disclosures. The authors declare no conflicts of interest.

Data availability. Data underlying the results presented in this paper are not publicly available at this time but may be obtained from the authors upon reasonable request.

Supplemental document. See Supplement 1 for supporting content.

REFERENCES

- X. Y. Bao and L. Chen, *Sensors* **12**, 8601 (2012).
- M. Soriano-Amat, H. F. Martins, V. Duran, L. Costa, S. Martin-Lopez, M. Gonzalez-Herraez, and M. R. Fernandez-Ruiz, *Light: Sci. Appl.* **10**, 51 (2021).
- A. Denisov, M. A. Soto, and L. Thevenaz, *Light: Sci. Appl.* **5**, e16074 (2016).
- A. D. Yan, S. Huang, S. Li, R. Z. Chen, P. Ohodnicki, M. Buric, S. W. Lee, M. J. Li, and K. P. Chen, *Sci. Rep.* **7**, 9360 (2017).
- K. P. Feng, J. W. Cui, D. Jiang, H. Dang, Y. H. Jin, X. Sun, Y. Z. Niu, and J. B. Tan, *Opt. Lett.* **43**, 3293 (2018).
- S. Y. Zhao, J. W. Cui, Z. J. Wu, Z. Y. Wang, and J. B. Tan, *J. Lightwave Technol.* **39**, 4101 (2021).
- C. H. Wang, K. Liu, Z. Y. Ding, J. F. Jiang, Z. E. Chen, Y. F. Feng, Y. Y. Zheng, Q. Q. Liu, and T. G. Liu, *J. Lightwave Technol.* **38**, 5825 (2020).
- X. Wang, R. Benedictus, and R. M. Groves, *Opt. Express* **29**, 19450 (2021).
- S. Loranger, M. Gagne, V. Lambin-Iezzi, and R. Kashyap, *Sci. Rep.* **5**, 11177 (2015).
- P. Lu, S. J. Mihailov, D. Coulas, H. M. Ding, and X. Y. Bao, *J. Lightwave Technol.* **37**, 4697 (2019).
- B. Redding, M. J. Murray, A. Donko, M. Beresna, A. Masoudi, and G. Brambilla, *Opt. Express* **28**, 14638 (2020).
- R. T. Cao, Y. Yang, M. H. Wang, X. R. Yi, J. Y. Wu, S. Huang, and K. P. Chen, *Opt. Lett.* **45**, 3163 (2020).
- C. B. Schaffer, A. O. Jamison, and E. Mazur, *Appl. Phys. Lett.* **84**, 1441 (2004).
- L. R. Rabiner, R. W. Schafer, and C. M. Rader, *IEEE Trans. Audio Electroacoust.* **17**, 86 (1969).